Exploring Mechanisms for Model-Dependency of the Stratospheric Response to Arctic Warming

Mudhar, Regan; Seviour, William J. M.; Screen, James A.; Geen, Ruth; Lewis, Neil T.; Thomson, Stephen I.

[Link to publication on Research at Birmingham portal](#)

Key Points:

- In a simple GCM, the sign and magnitude of the stratospheric polar vortex response to Arctic warming is highly sensitive to the basic state
- The stratospheric response also depends on the strength and vertical extent of Arctic warming in the troposphere
- Stronger/deeper warming narrows the lower stratospheric waveguide, slowing winds at lower levels than with weaker/shallower warming

Correspondence to:
R. Mudhar,
rm811@exeter.ac.uk

Exploring Mechanisms for Model-Dependency of the Stratospheric Response to Arctic Warming

Regan Mudhar[1] [iD], William J. M. Seviour[1,2] [iD], James A. Screen[1] [iD], Ruth Geen[3] [iD], Neil T. Lewis[1] [iD], and Stephen I. Thomson[1] [iD]

[1]Department of Mathematics and Statistics, University of Exeter, Exeter, UK, [2]Global Systems Institute, University of Exeter, Exeter, UK, [3]School of Geography, Earth and Environmental Sciences, University of Birmingham, Birmingham, UK

Abstract The Arctic is estimated to have warmed up to four times faster than the rest of the globe since the 1980s. There is significant interest in understanding the mechanisms by which such warming may impact weather and climate at lower latitudes. One such mechanism is the "stratospheric pathway"; Arctic warming is proposed to induce a wave-driven weakening of the stratospheric polar vortex, which may subsequently impact large-scale tropospheric circulation. However, recent comprehensive model studies have found systematic differences in both the magnitude and sign of the stratospheric response to Arctic warming. Using a series of idealized model simulations, we show that this response is sensitive to characteristics of the warming and mean polar vortex strength. In all simulations, imposed polar warming amplifies upward wave propagation from the troposphere, consistent with comprehensive models. However, as polar warming strength and depth increases, the region through which waves can propagate is narrowed, inducing wave breaking and deceleration of the flow in the lower stratosphere. Thus, the mid-stratosphere is less affected, with reduced sudden stratospheric warming frequency for stronger and deeper warming compared to weaker and shallower warming. We also find that the sign of the stratospheric response depends on the mean strength of the vortex, and that the stratospheric response in turn plays a role in the magnitude of the tropospheric jet response. Our results help explain the spread across multimodel ensembles of comprehensive climate models.

Plain Language Summary In the last four decades, the Arctic has warmed significantly faster than the rest of the world. Such warming has been suggested to generate waves in the atmosphere that move up into the stratosphere, where they break. If this were particularly powerful, it could disrupt and slow the typically strong and stable band of stratospheric winds encircling the winter pole, with potential consequences for surface weather and climate. However, state-of-the-art models disagree on how this "stratospheric polar vortex" responds to Arctic warming, even in terms of whether it will become weaker or stronger. In this study, our simplified climate model simulations indicate that the stratospheric response depends on certain characteristics of the Arctic warming. As it increases in strength and vertical extent, upward-moving waves are confined and forced to break lower down, resulting in fewer disruptions of the vortex above. We also find that the state of the vortex influences whether it weakens or strengthens, with implications for near-surface winds. Our results help explain the range of stratospheric responses simulated by more complex models.

1. Introduction

Over the past four decades, the Arctic has warmed up to four times faster than the rest of the globe (Rantanen et al., 2022). This "Arctic amplification" (AA) has been linked to apparent changes in observed northern mid-latitude winters, via modification of the tropospheric jet stream (Cohen et al., 2020; Francis & Vavrus, 2012). However, the exact mechanism for such a link remains unclear (Barnes & Screen, 2015). Some studies propose that this teleconnection may involve a stratospheric pathway, in which Arctic warming modulates upward-propagating planetary waves that weaken the stratospheric polar vortex (SPV) (Kretschmer et al., 2018; B. Kim et al., 2014). There is proposed to be a zonally asymmetric component to this warming, whereby regional warming generates Rossby waves at high latitudes (McKenna et al., 2018). Alternatively, the zonally symmetric component is proposed to weaken the equator-to-pole temperature gradient, whose impact on midlatitude circulation can modify upward-propagating waves: it is this component that we focus on in this study. With sufficiently strong wave-driving, this can raise the likelihood of sudden stratospheric warmings (SSWs), whose own anomalies can propagate downward and affect surface weather for weeks at a time (Baldwin et al., 2021; Kolstad

et al., 2010). Therefore, understanding potential changes in the SPV with Arctic warming is of both scientific and societal importance, but remains highly uncertain.

Recent studies show that the response of the SPV to climate change is model dependent. Several studies specifically investigate the SPV response to sea ice loss, or polar heating. Of these, idealized model simulations and multi-model means from more comprehensive studies typically show a vortex weakening with such forcings, though the latter is not robust. For example, analysis of Polar Amplification Model Intercomparison Project (PAMIP) simulations indicates a large inter-model spread in the stratospheric response to Arctic sea ice loss (Smith et al., 2022). Different models show changes in mean stratospheric winds of different magnitudes and even different signs. There is similar spread within more general climate change studies, such as CMIP5 and CMIP6 (Hall et al., 2021; Karpechko et al., 2022). The Arctic represents one source of uncertainty in SPV projections, which could propagate to uncertainty in the surface response (Liang et al., 2023; Zheng et al., 2023). However, few studies have investigated the extent to which model dependency in the SPV response to climate change is driven by model dependency in the response to Arctic climate change specifically. The range of stratospheric responses for the latter has been attributed to model differences, including in vertical resolution, model top, wave parameterization, and representation of dynamical processes (Kretschmer et al., 2020).

One driver of differences in simulated SPV response may be the differences in simulated temperature response to sea ice loss. Though observations indicate a winter warming extending to the upper troposphere (Screen & Simmonds, 2010; Screen et al., 2013), simulated Arctic warming in comprehensive climate models tends to be weaker and shallower (He et al., 2020). For example, in PAMIP sea ice loss is prescribed equally across all models, representing just one possible realization of future climate change (Smith et al., 2018). But due to model differences, some display a stronger and/or deeper warming response than others. Furthermore, the temperature response to sea ice loss in atmosphere-only model simulations is typically more muted and spatially confined than in fully-coupled models, as they underestimate poleward water vapor transport and vertical mixing (Deser et al., 2015; Xu et al., 2023).

Several studies propose that deep tropospheric warming may be key to resolving the mechanisms that link Arctic warming to midlatitude winter extremes (He et al., 2020; D. Kim et al., 2021; Labe et al., 2020; Sellevold et al., 2016; Xu et al., 2023). Their findings imply that the simulation of an unrealistically shallow temperature response to sea ice loss may underestimate the Arctic-midlatitude teleconnection. This includes the stratospheric pathway, as differences in the structure of atmospheric heating can influence winds and wave propagation. Thus, if models display a variety of temperature responses to sea ice loss, this may contribute to the range of simulated stratospheric responses.

Another potential reason for the range of stratospheric responses may be modeled differences in stratospheric climatology. The strength of the polar vortex modulates its own variability by impacting the ability of planetary waves to propagate vertically. In weak SPV states, vortex winds tend to be relatively steady, but slow. In contrast, a sufficiently strong SPV permits significant upward planetary wave propagation (Song & Robinson, 2004). With this comes mid-stratospheric wave breaking and SSWs; indicative of an "active" stratosphere. However, propagation of waves with lower wavenumbers becomes reduced as low-stratospheric winds accelerate. Then, increasingly strong mid-stratospheric zonal winds also require ever stronger forcings to generate the large-scale wave breaking necessary for the wind reversal of a SSW (Hall et al., 2021; Jucker et al., 2014). While some studies suggest that particularly strong anomalous tropospheric wave activity is sufficient to decelerate the SPV (Dunn-Sigouin & Shaw, 2020), others require a vortex that is structured to focus and even enhance upward wave activity (Albers & Birner, 2014). Thus, the strength and structure of simulated SPVs likely contributes to the magnitude or even sign of their response to forcings.

The two-way connection between the SPV and tropospheric circulation also means that uncertainty in the stratospheric response may exacerbate uncertainty in the tropospheric response. Many studies, including of observations, have linked stratospheric events to surface weather changes, with weak vortex events often associated with an equatorward shift of the tropospheric jet (Gerber & Polvani, 2009). The pattern of variability in both is comparable; in the troposphere, the "annular mode" pattern is a latitudinal fluctuation of the jet's position, and in the stratosphere a fluctuation of SPV strength (Kidston et al., 2015). Under active stratospheric conditions, the persistence of anomalies in the troposphere tends to increase, with eddy feedbacks considered key to this relationship (Butchart, 2022; Gerber & Polvani, 2009). Nevertheless, in a complex model study such as PAMIP, the sign of the tropospheric midlatitude jet response appears largely independent of that of the SPV. There is a

robust equatorward shift of the winter jet stream in response to future Arctic sea ice loss, in spite of the large inter-model spread in SPV response (Smith et al., 2022). This suggests minimal contribution from the stratospheric pathway. However other studies do highlight a role for the stratosphere in the near-surface response (B. Kim et al., 2014; Kretschmer et al., 2018; Labe et al., 2019; Xu et al., 2021). Some studies find weaker tropospheric responses to polar forcings when stratosphere-troposphere coupling is suppressed, as atmospheric anomalies generated during vortex strengthening or weakening events can interfere with near-surface circulation (Nakamura et al., 2016; Wu & Smith, 2016; Xu et al., 2023). Indeed, an active stratosphere has been associated with more persistent excursions of the jet (Gerber & Polvani, 2009), as well as a larger equatorward shift in response to polar warming (Wu & Smith, 2016).

Another way model uncertainty in the stratosphere can influence tropospheric uncertainty is through the stratospheric impact on tropospheric climatology. The climatological position of the jet informs the magnitude of the jet response to climate change forcings, with those that are located more equatorward tending to shift more (Garfinkel et al., 2013; Kidston & Gerber, 2010; McGraw & Barnes, 2016; Simpson & Polvani, 2016). This has been attributed to such a jet's greater persistence, through the fluctuation-dissipation theorem, as well as the strength of eddy-mean flow feedbacks (Garfinkel et al., 2013; McGraw & Barnes, 2016; Song & Robinson, 2004). Idealized model studies indicate a robust relationship between SPV strength and tropospheric jet location. Strong/weak SPVs are associated with more poleward/equatorward tropospheric jets (Chan & Plumb, 2009; Gerber & Polvani, 2009; Gerber et al., 2009; Polvani & Kushner, 2002), and Smith et al. (2022) propose climatological SPV strength as a weak emergent constraint on the tropospheric zonal wind response in PAMIP (in their Supplementary Figure 1). This suggests a mechanism by which a strong vortex state might cause the jet to occupy a position that makes it more susceptible to Arctic warming. Overall, differences in the mean strength of the SPV can influence the tropospheric response to polar heating in two ways; (a) through altering the SPV response to polar heating, and (b) through changing the tropospheric mean state and hence its sensitivity to forcing. The relative importance of these two mechanisms remains unclear.

In this study, we investigate the response of the stratosphere to polar heating in a dry idealized atmospheric GCM. The dynamics are driven by Netwonian relaxation to a prescribed equilibrium temperature profile in place of more complex radiative and convective schemes. We take this approach to isolate the dynamics from any uncertainties that may result from complex physical parameterizations, and because it allows us to explore parameter sensitivities in a relatively computationally inexpensive way. We aim to address three questions:

1. How does the stratospheric response to polar warming depend on characteristics of the warming, such as its strength and depth?
2. How does the stratospheric response to polar heating depend on the stratospheric mean state?
3. How does the tropospheric response to polar heating depend on the stratospheric mean state?

Idealized models have previously been used to study the stratosphere-troposphere connection (Gerber & Polvani, 2009; Lindgren et al., 2018; Polvani & Kushner, 2002), as well as climate change-representative thermal forcings, such as AA (Butler et al., 2010; Geen et al., 2023; Hassanzadeh et al., 2014; Wu & Smith, 2016), though often without a stratosphere. Taking an idealized modeling approach that includes an active stratosphere enables us to understand the fundamental mechanisms behind the modeled stratospheric response to polar heating and investigate the impact of model differences.

2. Methods

2.1. Model Configuration

We use the Isca modeling framework with a dry spectral dynamical core (Vallis et al., 2018), in which the temperature field is linearly relaxed to a zonally symmetric radiative equilibrium temperature profile, $T_{eq}(p, \phi)$ defined in pressure p and latitude ϕ, with Rayleigh friction for wind damping near the surface (Held & Suarez, 1994). $T_{eq} = T_{eq}^{trop}$ for $p \geq p_T$, and $T_{eq} = T_{eq}^{strat}$ for $p < p_T$, where,

$$T_{eq}^{trop} = \max\left[200\text{K}, (T_0 - \delta T_{\text{HS}})\left(\frac{p}{p_0}\right)^{\kappa}\right], \qquad (1)$$

Table 1

Values of Annular Mode Timescales for the First and Second Empirical Orthogonal Functions ($\tau_{1,2}$) and Their Proportionate Contribution to Overall Variance ($\nu_{1,2}$), Stratospheric Polar Vortex Mean ($U_{10,60}$) and Standard Deviation ($\sigma_{10,60}$), and Sudden Stratospheric Warming (SSW) Frequency, Including the 95% Confidence Interval

	Reanalysis	Control simulation
τ_1 (days)	16	24
ν_1 (%)	41	41
τ_2 (days)	10	16
ν_2 (%)	18	24
$U_{10,60}$ (m s^{-1})	30	47
$\sigma_{10,60}$ (m s^{-1})	16	27
SSWs (per 100 days)	0.45 ± 0.18	0.33 ± 0.09

Note. The control simulation is compared to analysis of daily ERA5 NDJF data (Hersbach et al., 2020).

in which $\delta T_{\text{HS}} = \Delta T_y \sin^2\phi + \Delta T_z \log(p/p_0) \cos^2\phi$, with the same meridional gradient (ΔT_y), vertical lapse rate (ΔT_z), surface pressure (p_0), and $\kappa = 2/7$ as in Held and Suarez (1994). T_{eq}^{strat} follows Polvani & Kushner (2002);

$$T_{eq}^{strat} = [1 - W(\phi)] \cdot T_{US}(p) + W(\phi) \cdot T_{US}(p_T)\left(\frac{p}{p_T}\right)^{-R\gamma/g}. \quad (2)$$

Through the weight function $W(\phi) = \frac{1}{2}\left(1 - \tanh\left[\frac{\phi-\phi_0}{\delta\phi}\right]\right)$, this profile smoothly transitions from one with a constant lapse rate of cooling (γ) over the winter pole to one that follows the U.S. Standard Atmosphere (T_{US}) in the summer hemisphere. Here, the values of the dry air gas constant (R) and gravitational constant (g), and parameters ϕ_0 and $\delta\phi$ are the same as in Polvani & Kushner (2002). However, the troposphere-stratosphere transition pressure is $p_T \sim 200$ hPa here, to address the bias in lower-stratospheric equilibrium temperatures (Jucker et al., 2013; Sheshadri et al., 2015). The strength of the generated Northern Hemisphere winter polar vortex is controlled by stratospheric polar temperatures, which are in turn controlled by γ, such that a larger γ induces stronger winds.

For our baseline, "control" simulation, we adjust model parameters to achieve a balance of relatively realistic jet annular mode timescales in the troposphere, with vortex strength and variability in the stratosphere. The stratospheric representation is key as we are investigating possible mechanisms behind the range of responses to polar heating recorded in more complex model studies. Furthermore, not significantly overestimating $\tau_{1,2}$ enables greater confidence that we will not also overestimate the magnitude of the response to any additional forcings, as per the fluctuation-dissipation theorem (Butler et al., 2010; Chan & Plumb, 2009; Ring & Plumb, 2008). Moving the transition pressure (p_T) lower and using $\gamma = 4$ K km^{-1} first generates semi-realistic $\tau_{1,2}$ (Table 1). Then, we introduce a constant wave-2 midlatitude heating perturbation (Figure 1b) to generate waves and achieve the relatively realistic $U_{10,60}$ and SSW frequency (Lindgren et al., 2018). This generates a climatology that is broadly consistent with reanalysis and similar studies (Lindgren et al., 2018; Ring & Plumb, 2007; Walz et al., 2023; Wu & Smith, 2016). The control simulation is compared to reanalysis in Table 1: we use NDJF zonal-mean zonal wind ERA5 data from 1979 to 2023 (Hersbach et al., 2020), with latitudinal resolution of 1° and 37 vertical levels up to 1 hPa. $\tau_{1,2}$ and $\nu_{1,2}$ are calculated from daily zonal winds between $p > 100$ hPa and $\phi > 20°$N (Dawson, 2016; Sheshadri & Plumb, 2017). The stratospheric variables, including SSW frequency, are calculated using daily zonal winds at 10 hPa, 60°N (Charlton & Polvani, 2007). We build on this control set-up for our experiments, with some of the possible limitations of our modeling approach discussed in Section 4.

To assess the response to polar heating, we impose a constant zonally symmetric thermal forcing at the northern polar surface,

$$Q(\phi,p) = A \cdot \frac{1}{2}\left[1 + \tanh\frac{p - p_{top}}{p_{th}}\right]\left(\frac{p_0 - p_{ref}}{p_0 - p_{top}}\right) \cdot \exp\left(-\frac{\phi + 90}{\phi_w}\right)^2, \quad (3)$$

following Orlanski and Solman (2010). We also include a scaling using p_{ref} to alter the heating magnitude as the vertical extent of the heating changes in order to ensure the same total energy input is applied for a given heating amplitude A (Geen et al., 2023). This enables easy comparison between simulations with different heating depths, as controlled by p_{top}. Our "default" polar heating set-up uses $A = 4$ K day^{-1}, $p_{top} = 600$ hPa, $\phi_w = 15°$, $p_{th} = 50$ hPa, $p_{ref} = 800$ hPa, and $p_0 = 1,000$ hPa, and is shown in Figure 1b. For experiments in which we test the dependency of the stratospheric response to polar heating on the vortex itself, we use this default polar heating and simply vary γ between 1 and 6 K km^{-1} (Equation 2). In experiments where we test the dependency on heating strength, we use $p_{top} = 600$ hPa and vary A between 0.5 and 8 K day^{-1}. Here, $A = 1$ K day^{-1} produces a ~3 K near-surface polar cap warming, comparable to the multi-model mean warming response to future Arctic sea ice loss in the atmosphere-only PAMIP simulations (Screen et al., 2022; Smith et al., 2022). For heating depth experiments, we use $A = 4$ K day^{-1} and vary p_{top} between 900 and 300 hPa, with the energy input scaled to match
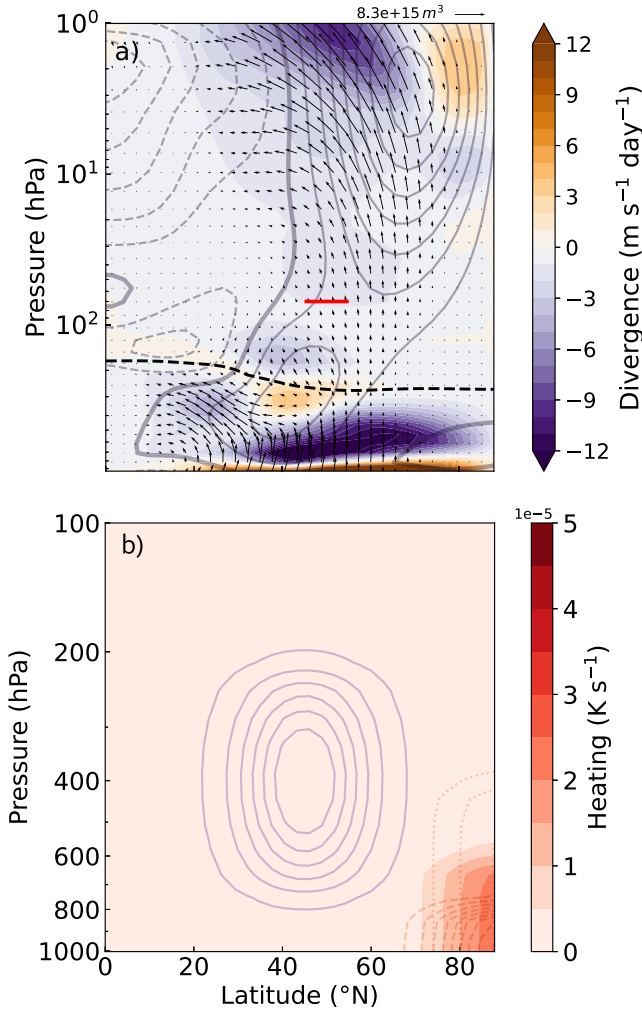
Figure 1. (a) The control simulation's Eliassen-Palm Flux (arrows, scaled following Jucker (2021)) and divergence (filled contours), overlaid with the climatological zonal wind (gray line contours). The thick gray line is the zero wind line, the dashed black line shows the location of the tropopause prior to additional forcing (calculated following the standard WMO definition), and the horizontal red line at 70 hPa highlights the "neck" region. (b) Default imposed polar heating (red filled contours) with $p_{top} = 600$ hPa. Overlaid red lines are examples of shallower ($p_{top} = 800$ hPa, dashed) and deeper ($p_{top} = 400$ hPa, dotted) set-ups. Purple solid lines indicate the location of the wave-2 midlatitude heating at 180°E, with maximum amplitude of $\sim 7 \times 10^{-5}$ K s^{-1} (i.e., 6 K day^{-1}, as in Lindgren et al. (2018)).

Table 2
Values of A and B, and the Form of P(ϕ) Used in Equation 4

Experiment	A	B	$P(\phi)$
J30	0	0	N.A.
	0	10	$\sin[4\phi - 45]$
J40	5	4	$\sin[4(\phi - 45)]$
	5	12	$\sin[4(\phi - 45)]$
J50	5	20	$\sin[4(\phi - 45)]$

Note. Experiments that align with those in Garfinkel et al. (2013) are labeled J30, J40, and J50.

the default case. Here, $p_{top} = 300$ hPa produces a polar cap warming of $\sim$13 K, slightly below that of CMIP6 simulations with SSP5-8.5 and abrupt 4×CO$_2$ forcings (Cai et al., 2021; Hu et al., 2022; Zhang et al., 2023).

To assess the tropospheric jet response dependency on tropospheric versus stratospheric factors, we replace δT_{HS} in Equation 1 with

$$
\begin{aligned}
\delta T_{new} = \delta T_{HS} &+ A \cos[2(\phi - 45)] \cdot P(\phi) \\
&+ B \cos[2(\phi - 45)] \cdot \sin[3(\phi - 60)] \\
&\times \left[\exp\left(-\frac{(\phi - 50)^2}{2 \cdot 15^2}\right) + \exp\left(-\frac{(\phi + 50)^2}{2 \cdot 15^2}\right) \right],
\end{aligned}
\tag{4}
$$

following Garfinkel et al. (2013). With this, we control the jet location by modifying tropospheric baroclinicity, via A, B and the form of $P(\phi)$ (Table 2). Doing so has minimal impact on the stratosphere, such that for simulations in Table 2 run with fixed $\gamma = 1$ K km^{-1}, SPV mean strength $U_{10,60}$ only varies between 20 and 28 m s^{-1} (see red triangles on Figure 7).

The model is run at spectral T42 horizontal resolution (64 × 128 lat-lon equivalent), with 40 vertical levels, and linear damping at the model top ($p < 0.5$ Pa, with 0.5 day^{-1} timescale). In Section 3, we analyze daily-average outputs from 40 years-long perpetual winter simulations ($\sim$160 winters).

2.2. Diagnostics

We look at the change in vortex mean winds and their variability across experiments, using the 10 hPa, 60°N zonal-mean zonal wind. We refer to the former with $U_{10,60}$, and for variability we use both standard deviation ($\sigma_{10,60}$) and SSW frequency, following Charlton and Polvani (2007). Throughout, we use refractive index squared to infer the structure of the atmospheric waveguide for planetary-scale waves, with wavenumber $k = 1$ (Matsuno, 1970). With the assumption of hydrostatic balance, we have derived an equation for n^2 from Equation 5 of Weinberger et al. (2021), which accounts for a spatially varying buoyancy frequency, $N^2(\phi, p)$;

$$
n^2 = a^2 M70n_{N_{\phi,p}},
\tag{5}
$$

where

$$
\begin{aligned}
M70n_{N_{\phi,p}} = \frac{\bar{q}_\phi}{a \cdot \bar{u}} &- \left(\frac{k}{a \cos \phi}\right)^2 - \frac{f^2}{N^2 H^2} \cdot \left[\frac{1}{4} - \frac{1}{N}\left(3p \frac{\partial N}{\partial p} + p^2 \frac{\partial^2 N}{\partial p^2}\right) \right. \\
&\left. + \frac{2p^2}{N^2}\left(\frac{\partial N}{\partial p}\right)^2\right].
\end{aligned}
\tag{6}
$$

We calculate n^2 using time- and zonal-mean zonal wind and temperature, where $\bar{u}$ is the zonal-mean zonal wind, a is the Earth's radius, H is the density scale height, $\bar{q}_\phi$ is the meridional gradient of potential vorticity (see, e.g., Simpson et al., 2009, for more detail), and

$$
N^2(\phi, p) = -\frac{Rp}{H^2} \cdot \frac{\partial T / \partial p - RT}{p c_p}.
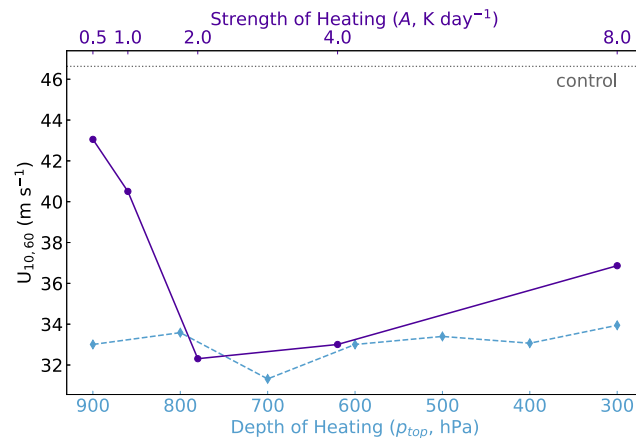\tag{7}
$$

Figure 2. $U_{10,60}$ in the strength (purple circles) and depth (blue diamonds) of polar heating experiments. The control experiment value in Table 1 is also shown in gray.

n^2 is, in part, dominated by zonal winds, and that in the "neck" region between the polar vortex and tropospheric westerlies is particularly key (indicated in red on Figure 1a, at 70 hPa, 45°N−55°N). Previous model studies link the strength of climatological winds in the neck region to the polar vortex response to increased CO_2 as such winds determine the ability of propagating waves to reach the mid-stratosphere (Sigmond & Scinocca, 2010). Additionally, a local maximum in buoyancy frequency around 200 hPa, 45°N–75°N also means that the final term in Equation 6 dominates n^2 in the so-called tropopause inversion layer, generating a region of negative n^2 there (Weinberger et al., 2021, 2022). Thus, refractive index can provide a clue to wave propagation, with areas of negative n^2 typically taken as barriers to flow. We also use Eliassen-Palm (EP) flux to indicate the direction of propagation of waves, and its divergence to understand wave breaking (EP flux convergence) (Andrews et al., 1983; Wu & Smith, 2016). In Section 3.3 we also look at the eddy-driven jet (EDJ), which is calculated as the time-mean of the maximum strength of the zonal-mean 850 hPa zonal wind (to the nearest grid point), and its location is the corresponding latitude of that maximum.

3. Results

In this section, we first examine the dependency of the SPV response to polar heating strength and depth, and then on climatological vortex strength. In all experiments, imposed polar heating enhances upward wave propagation from the troposphere, as in comprehensive model studies (Smith et al., 2022).

3.1. SPV Response Dependency on Polar Heating

The introduction of polar heating consistently weakens mean polar vortex winds (Figures 2 and 3), corroborating previous studies (Smith et al., 2022; Wu & Smith, 2016). Though predominantly on the equatorward side of the vortex, we find that the structure of that weakening depends on the strength and vertical extent of the heating. At lower values of A, $U_{10,60}$ becomes progressively weaker as the heating becomes stronger (Figure 2). However, increasing A beyond ~2 K day^{-1} has the effect of moving the weakening to lower levels (Figure 3c). The same change in the location of weakening is seen when changing p_{top}, though with smaller variation in $U_{10,60}$ (Figure 2). We also note that the simulations show a consistent equatorward shift of the tropospheric EDJ.

Notably, there is a significant change in vortex variability across experiments. Introducing polar heating reduces $\sigma_{10,60}$, which becomes increasingly low as both heating strength and depth increase. This is partly reflected in changes in SSW frequency (Figure 4). Weak heating does not significantly change SSW frequency compared to the control, as noted previously (Wu & Smith, 2016), but for moderate to strong heating ($A = 2 - 8$ K day^{-1}), SSW frequency falls in line with $\sigma_{10,60}$. Similarly, SSW frequency reduces from the shallowest to the deepest heating; the mid-stratosphere becomes less variable as the polar heating becomes stronger or extends to higher levels, with the region of strongest deceleration moving to low-stratospheric levels (Figures 4 and 3, respectively).
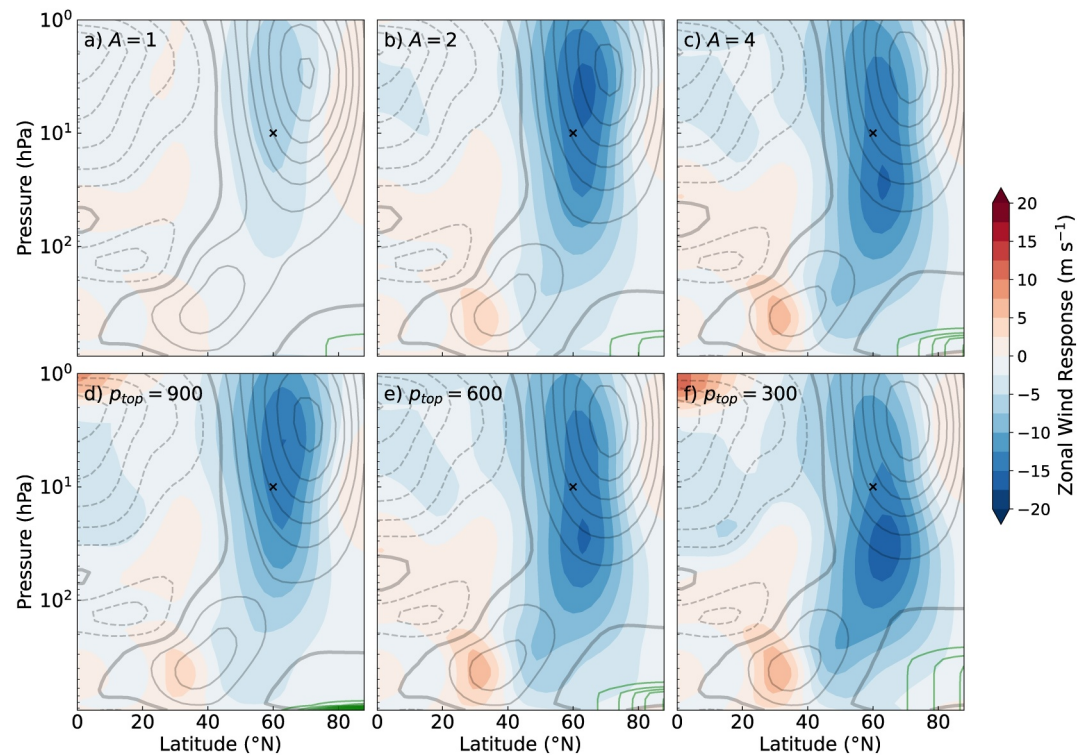
Figure 3. Time- and zonal-mean zonal wind response (filled contours) for (a–c) increasingly strong (A, K day^{-1}) and (d–f) increasingly deep (p_{top}, hPa) polar heating, overlaid with the polar heating experiment's zonal wind (gray line contours, 10 m s^{-1} interval). The thick gray line is the zero wind line, green line contours are the polar heating, and the crosses mark 10 hPa, 60°N.

Concurrently, the region of negative n^2 in the TIL is enhanced and neck winds decelerate, accompanied by a notable change in the zero-wind line poleward of 60°N. Introducing polar warming weakens the surface meridional temperature gradient and, via thermal wind balance, induces easterly zonal wind anomalies. Both increasing the strength of polar heating for a given depth and the depth for a given strength have the effect of further reducing the meridional temperature gradient in the upper troposphere. This allows the region of polar easterlies, extending up to ~400 hPa in our control, to reach further into the upper troposphere, reflected in the upward shift of the zero-wind line over the pole (Figure 3).

As polar heating extends polar easterlies and shifts the zero-wind line, the UTLS waveguide narrows and neck winds weaken (Figure 5). This modifies wave propagation. Near the surface, EP flux convergence is enhanced around 40°N (Figure 6), while in the upper troposphere, the region of EP flux divergence/convergence, likely generated by the wave-2 heating perturbation in the midlatitudes, is amplified by the polar forcing. As the polar heating becomes stronger and deeper, that amplification is enhanced (Figure 6), with stronger convergence suggesting an increase in UTLS wave breaking. These changes in EP flux are consistent with that in refractive index (cf. Simpson et al., 2009). In the deepest heating case, for example, not only is the region of negative n^2 stronger, but the regions of positive n^2, where waves can easily propagate, reduce—coinciding with that area of enhanced upper troposphere convergence (Figures 5f and 6f). EP flux convergence can be considered a measure of the easterly force exerted by waves on the zonal mean flow (Baldwin & Dunkerton, 2001; Holton & Hakim, 2013). Hence, the implied wave breaking is consistent with the deceleration of westerlies around the same region (Figure 3). Altogether, polar heating of increasing strength or vertical extent sufficiently modifies the waveguide to force upward propagating waves through an increasingly narrow UTLS neck. As a result, they break at lower levels, with the region of stratospheric zonal wind deceleration shifting lower. There is reduced upward wave propagation and the mid-stratosphere is relatively undisturbed; the polar vortex becomes less variable, with fewer wave breaking events there to trigger SSWs (Figure 4).
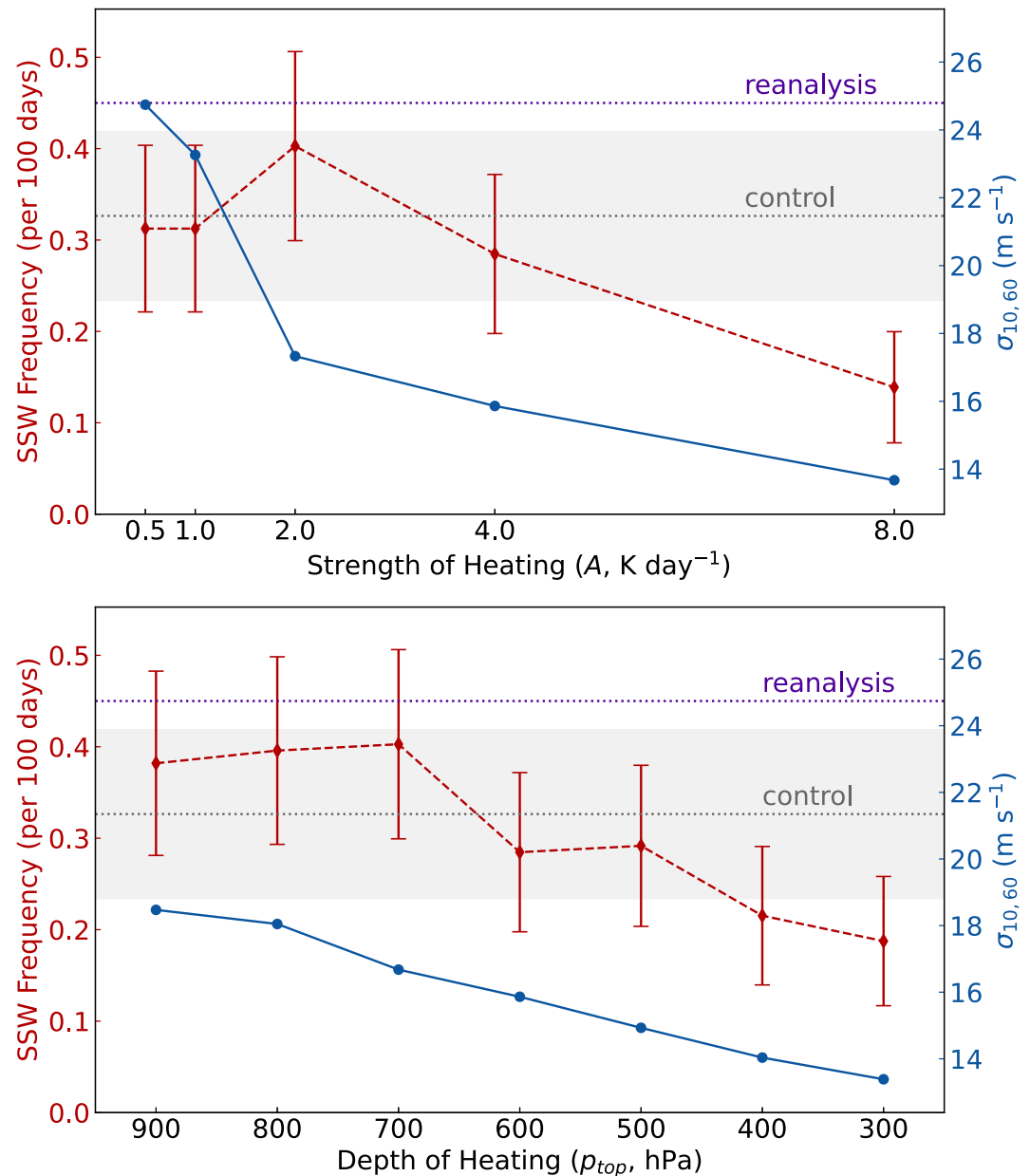
Figure 4. Sudden stratospheric warming (SSW) frequency (red triangles) and $\sigma_{10,60}$ (blue circles) for the (a) strength and (b) depth of heating experiments. For SSW frequency, the 95% confidence interval is indicated by the error bars. SSW frequency calculated from ERA5 data and the control experiment are also shown, with the latter's error shaded.

3.2. Stratospheric Response Dependency on Stratospheric State

We now consider how differences in the climatological strength of the SPV may impact its own response to polar warming. In our idealized model, changing the lapse rate of polar stratospheric cooling (γ), allows us to simulate polar vortices with a range of strengths that encompass that seen in PAMIP. As expected, without any polar heating, $U_{10,60}$ increases from 10 to 90 m s^{-1} as we increase γ (Figure 7) (Kushner & Polvani, 2004; Polvani & Kushner, 2002). Comparatively, $U_{10,60}$ ranges from ~20 to 45 m s^{-1} across the atmosphere-only PAMIP models' "present day" climatologies (Smith et al., 2022). Again, we note that the simulations show a consistent equatorward shift of the tropospheric EDJ.

In our idealized model, we introduce the default polar heating (Section 2.1) into this variety of climatologies and see different signed responses, as in complex models (Smith et al., 2022). Now, changing γ has a more muted
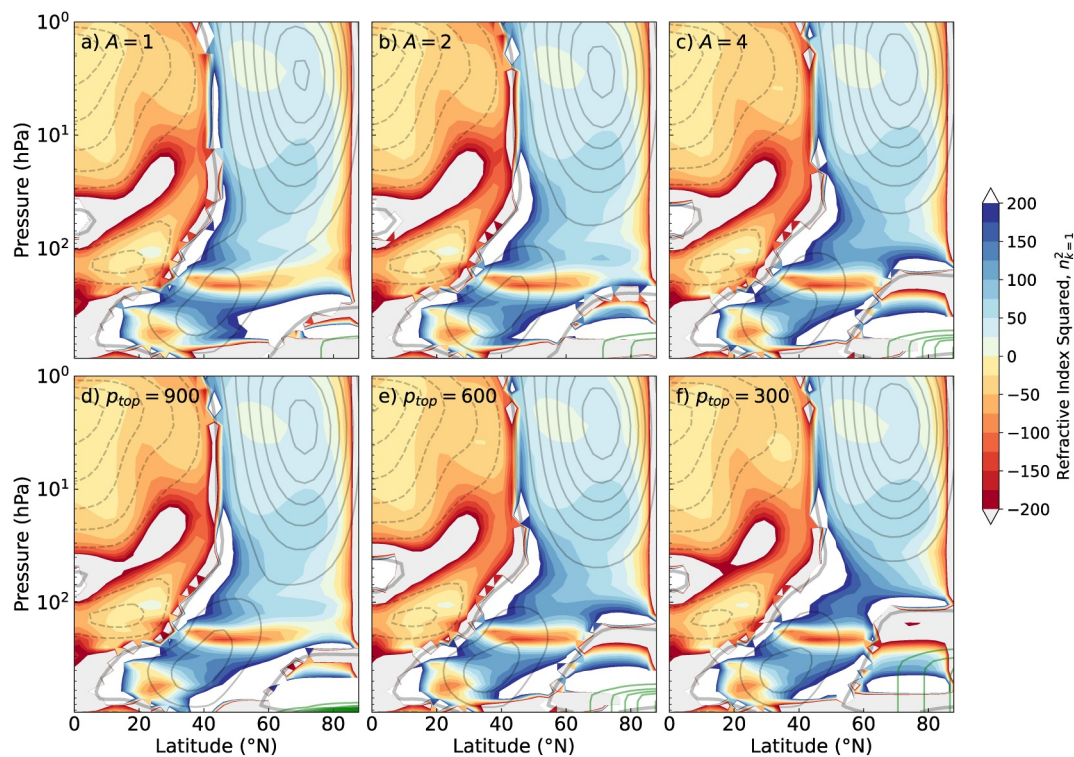
Figure 5. As in Figure 3, but filled contours are each experiment's time- and zonal-mean refractive index squared (i.e., not response).
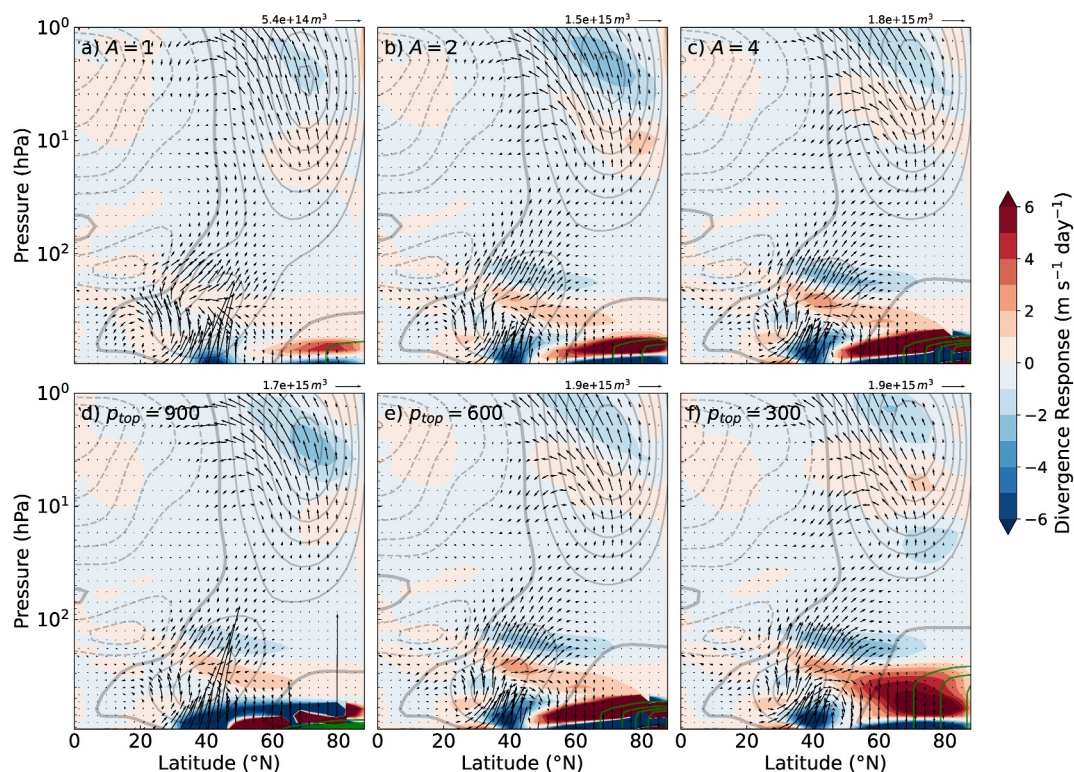

Figure 6. As in Figure 3, but filled contours are the time- and zonal-mean Eliassen-Palm (EP) flux divergence response to polar heating, overlaid with response in EP flux arrows.
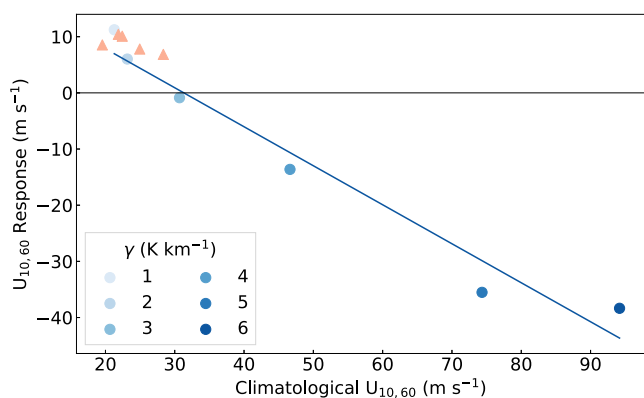
Figure 7. Differences in $U_{10,60}$ response to polar heating for simulations with different climatological stratospheric states (blue circles). Points are plotted as a function of the mean strength of $U_{10,60}$ in experiments without polar heating, with the increasing darkness indicating increasing lapse rate of polar stratospheric cooling (γ, see legend). This is plotted against the response to the default polar heating; that is, difference relative to the climatology. The red triangles are for the modified T_{eq} experiments, which use $\gamma = 1$ K km^{-1}.

response (Figure 8); $U_{10,60}$ ranges from 30 to 50 m s^{-1}. With the lowest γ, the stratosphere cools in response to polar heating (not shown), causing the vortex to strengthen (Figure 8a). This strengthening is greatest for $\gamma = 1$ K km^{-1}, with $\gamma = 3$ K km^{-1} showing minimal response to polar heating. For $\gamma = 4$ K km^{-1} and higher, polar heating leads to a warming in the stratosphere that causes a weakening (and narrowing) of the SPV (Figure 8c). When γ is low, vortex winds are weak and the SPV is essentially isolated from the troposphere (Figure 9a). Waves therefore struggle to propagate up and the SPV is steady, with few SSWs (not shown); a "passive" stratosphere. Introducing polar heating then has two effects. It amplifies upward wave propagation from the troposphere (Figure 10) but also causes the extension of polar easterlies, with weaker neck winds and an eroded waveguide (as in Section 3.1); the upper tropospheric region of negative n^2 is strengthened and areas of positive n^2 reduce. Thus, despite there being more activity, waves are less able to propagate into the stratosphere (Figure 10a). The vortex then becomes less disturbed than it already was, strengthening as a result (Figure 8a). Alternatively, when the SPV is sufficiently strong, there is a better connection to the troposphere (Song & Robinson, 2004). Moderately strong neck winds enhance the waveguide, allowing more waves into the stratosphere: the upper tropospheric region of negative n^2 does not significantly change with increasing γ, but the areas of positive n^2 are extended. As a result, the SPV is stronger but also more variable, with a higher frequency of SSWs—up to a point. Too strong a vortex reflects planetary waves, however, with an accompanying lower frequency of SSWs (Hall et al., 2021; Jucker et al., 2014; Perlwitz & Harnik, 2004). In a sufficiently active stratosphere, introducing polar heating again has two effects, but this time a different outcome. As before, it causes a narrowing of the neck. However, due to the relatively greater strength of mid- to low-stratospheric winds, it is insufficient to significantly erode the waveguide (Figure 9f). As a result, the polar heating-driven increase in wave activity is able to propagate into the stratosphere, and there is enhanced wave breaking (flux convergence) and strong deceleration of winds within the vortex (Figures 10c and 8c, respectively). Altogether, we see a greater deceleration of the polar vortex in response to polar heating when westerlies are stronger throughout the climatological stratosphere. Such a vortex seems to permit wave activity upward into the stratosphere and enable stronger wave-mean flow interactions (Albers & Birner, 2014), resulting in a greater deceleration of winds in the SPV itself.

3.3. Tropospheric Response Dependency on the Stratospheric State

We can use the γ experiments to understand how differences in the climatological strength of the SPV may impact the tropospheric response to polar warming. Regardless of the strength of the mean stratospheric zonal winds or
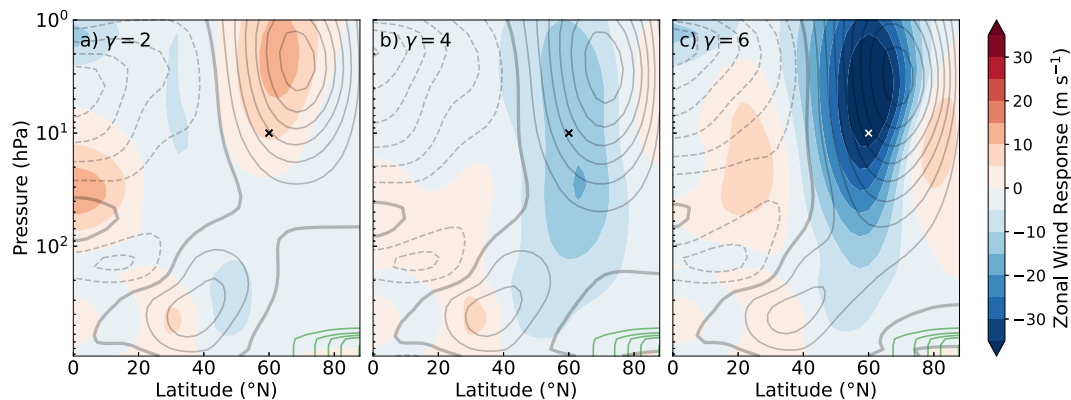
Figure 8. Time- and zonal-mean zonal wind response to polar heating (filled contours, with a different colourbar than in Figure 3) with (a–c) increasingly strong polar stratospheric lapse rate (γ, K km^{-1}), overlaid with the polar heating experiment's zonal wind (gray line contours, 10 m s^{-1} interval). The thick gray line is the zero wind line, green line contours are the polar heating, and the crosses mark 10 hPa, 60°N.
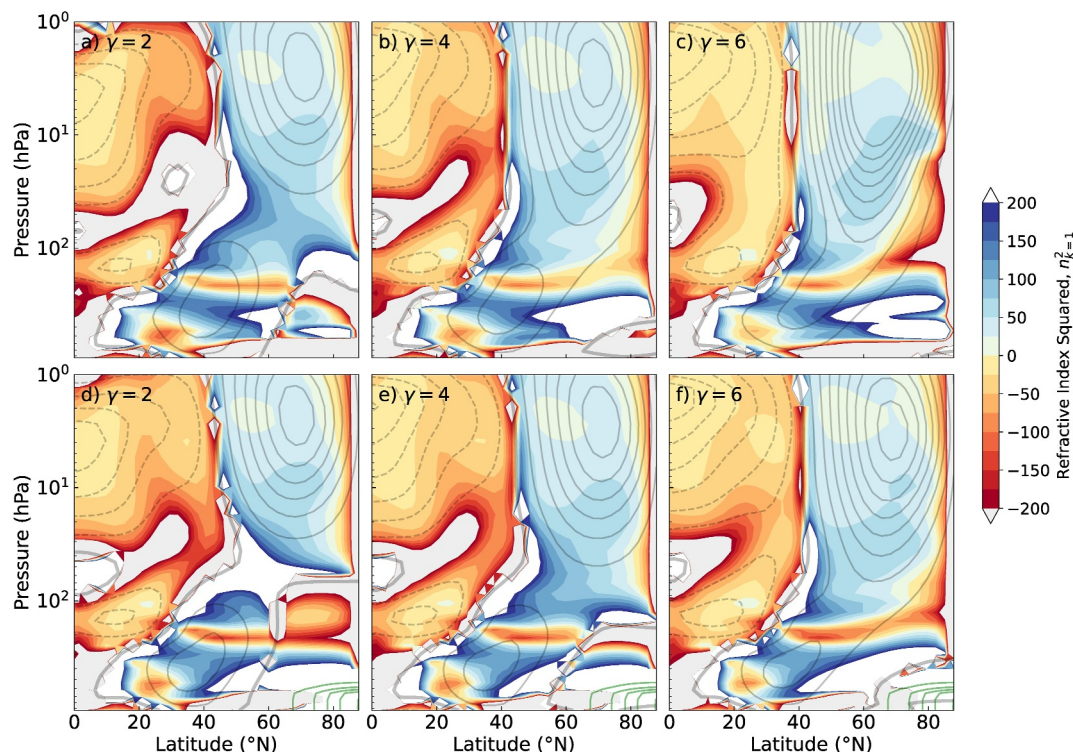
Figure 9. As in Figure 8, but filled contours are each experiment's time- and zonal-mean refractive index squared (i.e., not response), such that (a–c) and (d–f) are without and with polar heating, respectively.

the sign of their response, introducing polar heating results in an equatorward shift of the EDJ (Figure 8), consistent with both complex and idealized model studies (Butler et al., 2010; Smith et al., 2022). Without polar heating, increasing γ marginally weakens the EDJ and causes it to shift more poleward overall (Figure 11). With polar heating, the response to modifying γ is more constrained; the EDJ moves poleward by at most 1° compared to ∼3° without. This direction of change is consistent with previous studies (Gerber & Polvani, 2009; Kushner & Polvani, 2004; Polvani & Kushner, 2002), though the magnitude is lower. This is likely due to our use of the midlatitude heating perturbation, which has been noted to constrain jet variability (Garny et al., 2020). The equatorward jet shift has previously been attributed to a temperature gradient-driven modification of the region of lower-level baroclinic instability and thus meridional heat flux (McGraw & Barnes, 2016; Wu & Smith, 2016). We find that this response in EDJ location becomes larger with γ; for $\gamma = 1$ K km^{-1}, the shift is ∼4°, and for
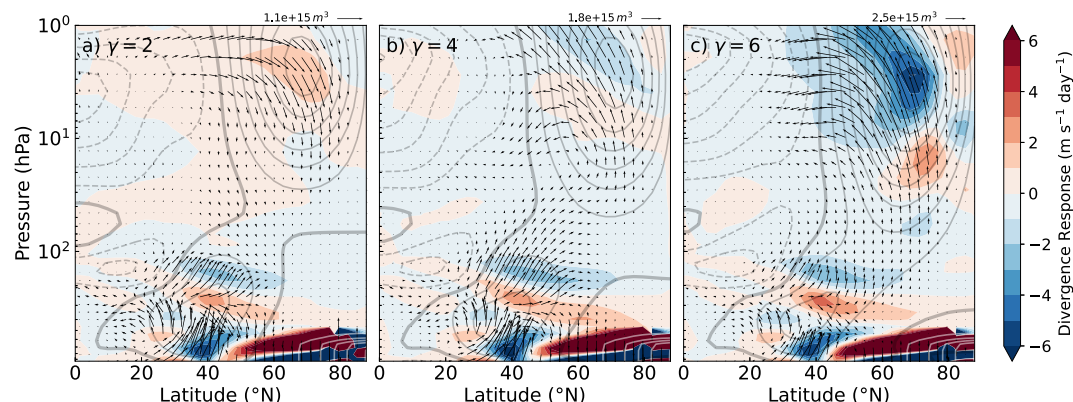

Figure 10. As in Figure 8, but filled contours are the time- and zonal-mean Eliassen-Palm (EP) flux divergence response to polar heating, overlaid with response in EP flux arrows.
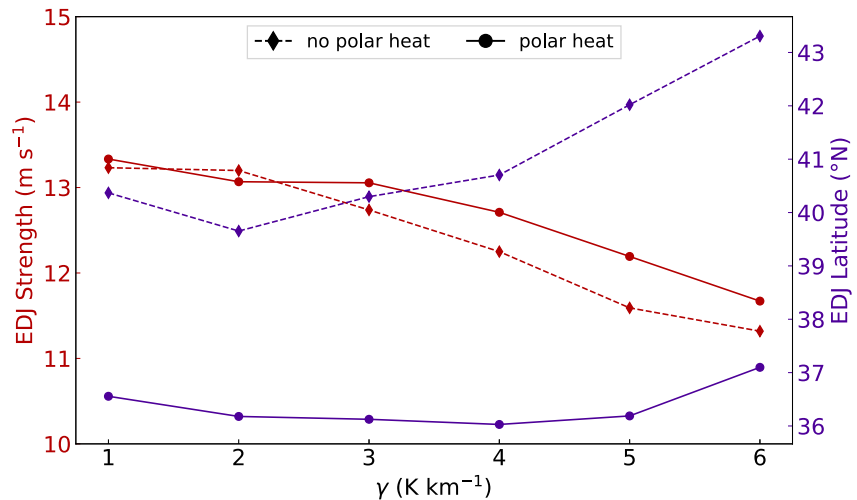
Figure 11. Eddy-driven jet (EDJ) strength (red) and latitude (purple) for experiments with an increasingly strong vortex without (diamonds) and with (circles) polar heating.

6 K km^{-1} is ~6°. Thus, we have a greater response to polar heating in both the SPV strength and the EDJ latitude with increasing γ. This suggests two ways in which the jet latitude response might be informed by the stratosphere. The first is that a sufficiently large γ can result in a more active stratosphere that therefore has a stronger response to polar heating. This manifests as an enhanced mid-stratospheric zonal wind deceleration and wave activity (Figures 8c and 10c, respectively), with a higher resultant SSW frequency. Thus with more stratospheric anomalies propagating back to the surface, the effect may be to shift the EDJ more equatorward. The second is that stratospheric climatology may influence the tropospheric response by changing the tropospheric mean state, including the mean jet latitude. We find that a stronger vortex is accompanied by a more poleward EDJ (Figure 11). But additionally, the polar heating-generated wave source in Figure 10 is constant in all experiments while the region in which waves can easily propagate changes—along with the zero-wind line, as seen in Figure 9. This suggests that a stronger climatological vortex induces a more poleward jet that is closer to, or even in, the direct region of influence of our polar forcing, which may cause that greater jet response.

To distinguish between these two possible pathways, we use a constant $\gamma = 1$ K km^{-1}, with the wave-2 heating perturbation, and modify the near-surface temperature profile via Equation 4 to separately control the EDJ location (Garfinkel et al., 2013). With this γ value we can span the range of EDJ locations in experiments in Section 3.2 by changing T_{eq}, which does not notably alter the stratospheric state (see the red triangles on Figure 7). These experiments investigate the sensitivity of the jet response to mean jet latitude, described by the slope of the red dashed line in Figure 12. This is compared to experiments that modified γ, with the slope of the blue solid line in the figure indicating the sensitivity of the jet response to polar vortex state, which influences both mean jet latitude and the polar vortex response. If the size of the jet response depended only on the jet location, we might expect comparable slopes between T_{eq} and γ experiments. The differences in the slopes indicate that both mechanisms discussed above play a role. That is, the stratospheric mean state influences the jet response to polar heating, both by changing the stratospheric response, and by changing the mean tropospheric jet latitude.

4. Discussion and Conclusions

We investigated the dependency of the stratospheric response to polar heating on characteristics of the heating and on the stratospheric mean state. We found that with a moderately strong polar vortex, surface polar heating consistently weakens stratospheric westerlies. The structure of that weakening, as well as the change in variability of the vortex, depends on the strength and vertical extent of the heating. The reduction in variability manifested as an overall lower SSW frequency. While the experiments varying strength and depth of warming all showed a weaker vortex, the sign of the vortex response was also found to be dependent on its mean state. With a weaker climatological vortex, polar heating narrowed the neck to limit wave propagation into an already passive stratosphere. With a moderately strong climatological vortex, the stratosphere was more active and then the
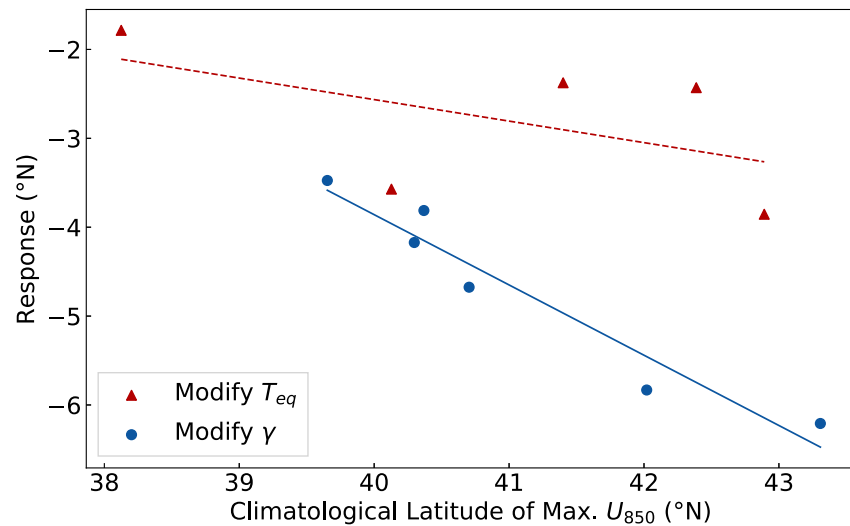
Figure 12. Climatological eddy-driven jet (EDJ) latitude in experiments without polar heating compared to its response to polar heating. The climatological jet location is modified in two different ways: through the tropospheric temperature profile (red triangles), via δT_{new} in Equation 4, and the stratospheric state (blue circles), via γ in Equation 2.

heating was not sufficient to restrict upward wave propagation. Indeed, the enhancement of wave activity by the imposed polar heating led to greater wave breaking and deceleration of flow in the mid-stratosphere.

We aimed for our idealized model configuration to be sufficiently realistic, so that we might use our results to explain the range of responses in comprehensive model studies, such as PAMIP. However, we acknowledge that it does make some significant simplifications. For example, we used 40 vertical levels and a horizontal resolution of T42, while most PAMIP models have over 50 levels and run at resolutions ranging from the equivalent of T63 to T255 (Smith et al., 2022). With our model, we found that a greater horizontal resolution of T85 induced a stratospheric state, and therefore responses to polar heating, that were comparable to the T42, $\gamma = 5$ simulations in Section 3.2, with a stronger climatological SPV. Increasing vertical resolution to 60 levels, meanwhile, did not significantly change climatology nor the subsequent stratospheric response to polar heating, though did notably overestimate τ_1. Ultimately, our conclusions do not qualitatively change with higher resolution, and comparatively more expensive, configurations. Furthermore, unlike PAMIP and the real atmosphere, we do not have realistic continents or topography to force stationary waves. To induce stratospheric variability, we instead used an idealized wave-2 heating perturbation. Following Lindgren et al. (2018) for this meant that the top of the heating perturbation was at 200 hPa. This put some of the wave source above the tropopause, which is ∼300 hPa in the mid-to-high latitudes in our Polvani-Kushner simulation prior to additional forcing (Figure 1a). This could be considered unrealistic, but we found less than 4% of the heating perturbation's total heat input was above the tropopause. Additional experiments using a heating perturbation with a lower vertical extent, keeping it entirely below the tropopause, saw a 3% reduction in upward EP flux through 100 hPa, 40°N–60°N and gave a qualitatively similar response to imposed polar heating, as well as to changing the depth of the polar heating (not shown). This midlatitude heating perturbation approach has also previously been noted to unrealistically restrict the latitudinal variability of the free tropospheric jet under changing vortex strengths (Garny et al., 2020; Walz et al., 2023). The EDJ in our simulation with, compared to without, the heating perturbation was indeed more equatorward EDJ, but neither were as poleward nor as variable as in reanalysis. An alternative approach may have been to use topographic forcing, but in simulations with a 4,000 m wave-2 topography (Gerber & Polvani, 2009), we found unrealistically long τ_1 and low SSW frequencies (not shown). Furthermore, some studies have noted a similar effect on jet latitude with the topographic as with the thermal forcing (Gerber & Polvani, 2009; Lindgren et al., 2018). Since our aim was not to perfectly recreate observed climatology, but to have an experimental set-up in which to investigate the sensitivity of the SPV response to polar heating, we favored using the heating perturbation, as it was the wave source that helped us achieve this.

We suggest that the range of stratospheric responses seen in more complex models is unsurprising when viewed in the context of our much more simplified model experiments. The PAMIP models, for example, appear to differ in

the strength and depth of their warming response to Arctic sea ice loss, as well as displaying a range of vortex climatologies. Though our default polar heating is notably stronger than the warming induced by sea ice loss in PAMIP simulations (see Section 2.1), the response in the mean SPV strength and EDJ latitude in PAMIP is still weaker than in our experiment with an almost equivalent near-surface polar cap temperature response ($A = 1$ K day^{-1}, Figure 3a): this may, in part, be due to the influence of the stronger SPV. Nevertheless, we believe that to fully understand the impact of systematically changing the depth or strength of "heating" associated with AA in complex models would require additional analysis, or even specialized experiments, that are beyond the scope of our study. On the other hand, the PAMIP models simulate present day $U_{10,60} = 20$–45 m s^{-1} (see Smith et al., 2022, Supplementary Figure 1). Our control simulation, using $\gamma = 4$ K km^{-1}, produces $U_{10,60}$ within the spread of the PAMIP models, and by varying γ between 1 and 4 K km^{-1}, we generate a similar range ($U_{10,60} = 21$−47 m s^{-1}). Though our control simulation's SPV is on the stronger side, it has the benefit of additionally achieving relatively realistic tropospheric and stratospheric variability, as discussed above. Overall, we were able to change vortex strength within the range of the PAMIP models and found a similarly wide variety of vortex responses. Thus, whether a complex model has a more passive or active stratosphere, depending on the vortex strength, could explain the magnitude or even sign of simulated vortex response. But the different PAMIP models also have equatorward jet shifts of varying magnitudes in response to sea ice loss. While the sign of the jet shift is likely controlled by tropospheric processes, our experiments have shown that the magnitude may be modulated by the stratosphere. We suggest that the stratospheric state is important for the tropospheric response because it both influences the tropospheric climatology and the size of the vortex response, which modulates that of the jet too.

Data Availability Statement

Simulations were run with the Isca modeling framework (Vallis et al., 2018, available to install at https://github.com/ExeClim/Isca); the specific commit used has DOI: https://doi.org/10.5281/zenodo.10117892. EOFs calculated using the eofs python package (DOI: https://doi.org/10.5281/zenodo.594643) (Dawson, 2016). Refractive index and EP flux diagnostics were calculated using the aostools python package (DOI: https://doi.org/10.5281/zenodo.597598), with the latter plotted following Jucker (2021). ERA5 reanalysis data are freely available from the European Centre for Medium-Range Weather Forecasts (Hersbach et al., 2020, https://cds.climate.copernicus.eu/#!/search?text=ERA5&type=dataset).

References

Albers, J. R., & Birner, T. (2014). Vortex preconditioning due to planetary and gravity waves prior to sudden stratospheric warmings. *Journal of the Atmospheric Sciences*, *71*(11), 4028–4054. https://doi.org/10.1175/JAS-D-14-0026.1

Andrews, D. G., Mahlman, J. D., & Sinclair, R. W. (1983). Eliassen-palm diagnostics of wave-mean flow interaction in the GFDL "SKYHI" general circulation model. *Journal of the Atmospheric Sciences*, *40*(12), 2768–2784. https://doi.org/10.1175/1520-0469(1983)040⟨2768:ETWATM⟩2.0.CO;2

Baldwin, M. P., Ayarzagüena, B., Birner, T., Butchart, N., Butler, A. H., Charlton-Perez, A. J., et al. (2021). Sudden stratospheric warmings. *Reviews of Geophysics*, *59*(1), e2020RG000708. https://doi.org/10.1029/2020RG000708

Baldwin, M. P., & Dunkerton, T. J. (2001). Stratospheric harbingers of anomalous weather regimes. *Science*, *294*(5542), 581–584. https://doi.org/10.1126/science.1063315

Barnes, E. A., & Screen, J. A. (2015). The impact of Arctic warming on the midlatitude jet-stream: Can it? Has it? Will it? *Wiley Interdisciplinary Reviews: Climate Change*, *6*(3), 277–286. https://doi.org/10.1002/wcc.337

Butchart, N. (2022). The stratosphere: A review of the dynamics and variability. *Weather and Climate Dynamics*, *3*(4), 1237–1272. https://doi.org/10.5194/wcd-3-1237-2022

Butler, A. H., Thompson, D. W., & Heikes, R. (2010). The steady-state atmospheric circulation response to climate change-like thermal forcings in a simple general circulation model. *Journal of Climate*, *23*(13), 3474–3496. https://doi.org/10.1175/2010JCLI3228.1

Cai, S., Hsu, P. C., & Liu, F. (2021). Changes in polar amplification in response to increasing warming in CMIP6. *Atmospheric and Oceanic Science Letters*, *14*(3), 100043. https://doi.org/10.1016/j.aosl.2021.100043

Chan, C. J., & Plumb, R. A. (2009). The response to stratospheric forcing and its dependence on the state of the troposphere. *Journal of the Atmospheric Sciences*, *66*(7), 2107–2115. https://doi.org/10.1175/2009JAS2937.1

Charlton, A. J., & Polvani, L. M. (2007). A new look at stratospheric sudden warmings. Part I: Climatology and modeling benchmarks. *Journal of Climate*, *20*(3), 449–469. https://doi.org/10.1175/JCLI3996.1

Cohen, J., Zhang, X., Francis, J., Jung, T., Kwok, R., Overland, J., et al. (2020). Divergent consensuses on Arctic amplification influence on midlatitude severe winter weather. *Nature Climate Change*, *10*(1), 20–29. https://doi.org/10.1038/s41558-019-0662-y

Dawson, A. (2016). Eofs: A library for EOF analysis of meteorological, oceanographic, and climate data [Software]. *Journal of Open Research Software*, *4*(1), 14. https://doi.org/10.5334/jors.122

Deser, C., Tomas, R. A., & Sun, L. (2015). The role of ocean-atmosphere coupling in the zonal-mean atmospheric response to Arctic sea ice loss. *Journal of Climate*, *28*(6), 2168–2186. https://doi.org/10.1175/JCLI-D-14-00325.1

Dunn-Sigouin, E., & Shaw, T. (2020). Dynamics of anomalous stratospheric eddy heat flux events in an idealized model. *Journal of the Atmospheric Sciences*, *77*(6), 2187–2202. https://doi.org/10.1175/JAS-D-19

Francis, J. A., & Vavrus, S. J. (2012). Evidence linking Arctic amplification to extreme weather in mid-latitudes. *Geophysical Research Letters*, *39*(6), L06801. https://doi.org/10.1029/2012GL051000

Garfinkel, C. I., Waugh, D. W., & Gerber, E. P. (2013). The effect of tropospheric jet latitude on coupling between the stratospheric polar vortex and the troposphere. *Journal of Climate*, *26*(6), 2077–2095. https://doi.org/10.1175/JCLI-D-12-00301.1

Garny, H., Walz, R., Nützel, M., & Birner, T. (2020). Extending the modular earth submodel system (MESSY v2.54) model hierarchy: The ECHAM/MESSY idealized (EMIL) model setup. *Geoscientific Model Development*, *13*(11), 5229–5257. https://doi.org/10.5194/gmd-13-5229-2020

Geen, R., Thomson, S. I., Screen, J. A., Blackport, R., Lewis, N. T., Mudhar, R., et al. (2023). An explanation for the metric dependence of the midlatitude jet-waviness change in response to polar warming. *Geophysical Research Letters*, *50*(21), e2023GL105132. https://doi.org/10.1029/2023gl105132

Gerber, E. P., Orbe, C., & Polvani, L. M. (2009). Stratospheric influence on the tropospheric circulation revealed by idealized ensemble forecasts. *Geophysical Research Letters*, *36*(24), L24801. https://doi.org/10.1029/2009GL040913

Gerber, E. P., & Polvani, L. M. (2009). Stratosphere-troposphere coupling in a relatively simple AGCM: The importance of stratospheric variability. *Journal of Climate*, *22*(8), 1920–1933. https://doi.org/10.1175/2008JCLI2548.1

Hall, R. J., Mitchell, D. M., Seviour, W. J., & Wright, C. J. (2021). Persistent model biases in the CMIP6 representation of stratospheric polar vortex variability. *Journal of Geophysical Research: Atmospheres*, *126*(12), e2021JD034759. https://doi.org/10.1029/2021JD034759

Hassanzadeh, P., Kuang, Z., & Farrell, B. F. (2014). Responses of midlatitude blocks and wave amplitude to changes in the meridional temperature gradient in an idealized dry GCM. *Geophysical Research Letters*, *41*(14), 5223–5232. https://doi.org/10.1002/2014GL060764

He, S., Xu, X., Furevik, T., & Gao, Y. (2020). Eurasian cooling linked to the vertical distribution of Arctic warming. *Geophysical Research Letters*, *47*(10), e2020GL087212. https://doi.org/10.1029/2020GL087212

Held, I. M., & Suarez, M. J. (1994). A proposal for the intercomparison of the dynamical cores of atmospheric general circulation models. *Bulletin of the American Meteorological Society*, *75*(10), 1825–1830. https://doi.org/10.1175/1520-0477(1994)075<1825:apftio>2.0.co;2

Hersbach, H., Bell, B., Berrisford, P., Hirahara, S., Horányi, A., Muñoz-Sabater, J., et al. (2020). The ERA5 global reanalysis [Dataset]. *Quarterly Journal of the Royal Meteorological Society*, *146*(730), 1999–2049. https://doi.org/10.1002/qj.3803

Holton, J. R., & Hakim, G. J. (2013). *An introduction to dynamic meteorology* (5th ed., Vol. 88). Academic Press. https://doi.org/10.1016/c2009-0-63394-8

Hu, X., Liu, Y., Kong, Y., & Yang, Q. (2022). A quantitative analysis of the source of inter-model spread in Arctic surface warming response to increased CO_2 concentration. *Geophysical Research Letters*, *49*(18), e2022GL100034. https://doi.org/10.1029/2022GL100034

Jucker, M. (2021). Scaling of Eliassen-Palm flux vectors [Software]. *Atmospheric Science Letters*, *22*(4), e1020. https://doi.org/10.1002/asl.1020

Jucker, M., Fueglistaler, S., & Vallis, G. K. (2013). Maintenance of the stratospheric structure in an idealized general circulation model. *Journal of the Atmospheric Sciences*, *70*(11), 3341–3358. https://doi.org/10.1175/JAS-D-12-0305.1

Jucker, M., Fueglistaler, S., & Vallis, G. K. (2014). Stratospheric sudden warmings in an idealized GCM. *Journal of Geophysical Research*, *119*(19), 054-11. https://doi.org/10.1002/2014JD022170

Karpechko, A. Y., Afargan-Gerstman, H., Butler, A. H., Domeisen, D. I. V., Kretschmer, M., Lawrence, Z., et al. (2022). Northern Hemisphere stratosphere-troposphere circulation change in CMIP6 models: 1. Inter-model spread and scenario sensitivity. *Journal of Geophysical Research: Atmospheres*, *127*(18), e2022JD036992. https://doi.org/10.1029/2022jd036992

Kidston, J., & Gerber, E. P. (2010). Intermodel variability of the poleward shift of the austral jet stream in the CMIP3 integrations linked to biases in 20th century climatology. *Geophysical Research Letters*, *37*(9), L09708. https://doi.org/10.1029/2010GL042873

Kidston, J., Scaife, A. A., Hardiman, S. C., Mitchell, D. M., Butchart, N., Baldwin, M. P., & Gray, L. J. (2015). Stratospheric influence on tropospheric jet streams, storm tracks and surface weather. *Nature Geoscience*, *8*(6), 433–440. https://doi.org/10.1038/NGEO2424

Kim, B., Son, S. W., Min, S. K., Jeong, J. H., Kim, S. J., Zhang, X., et al. (2014). Weakening of the stratospheric polar vortex by Arctic sea-ice loss. *Nature Communications*, *5*(1), 4646. https://doi.org/10.1038/ncomms5646

Kim, D., Kang, S. M., Merlis, T. M., & Shin, Y. (2021). Atmospheric circulation sensitivity to changes in the vertical structure of polar warming. *Geophysical Research Letters*, *48*(19), e2021GL094726. https://doi.org/10.1029/2021GL094726

Kolstad, E. W., Breiteig, T., & Scaife, A. A. (2010). The association between stratospheric weak polar vortex events and cold air outbreaks in the Northern Hemisphere. *Quarterly Journal of the Royal Meteorological Society*, *136*(649), 886–893. https://doi.org/10.1002/qj.620

Kretschmer, M., Coumou, D., Agel, L., Barlow, M., Tziperman, E., & Cohen, J. D. (2018). More-persistent weak stratospheric polar vortex states linked to cold extremes. *Bulletin of the American Meteorological Society*, *99*(1), 49–60. https://doi.org/10.1175/BAMS-D-16-0259.1

Kretschmer, M., Zappa, G., & Shepherd, T. G. (2020). The role of Barents–Kara sea ice loss in projected polar vortex changes. *Weather and Climate Dynamics*, *1*(2), 715–730. https://doi.org/10.5194/wcd-1-715-2020

Kushner, P. J., & Polvani, L. M. (2004). Stratosphere-troposphere coupling in a relatively simple AGCM: The role of eddies. *Journal of Climate*, *17*(3), 629–639. https://doi.org/10.1175/1520-0442(2004)017⟨0629:SCIARS⟩2.0.CO;2

Labe, Z., Peings, Y., & Magnusdottir, G. (2019). The effect of QBO phase on the atmospheric response to projected Arctic sea ice loss in early winter. *Geophysical Research Letters*, *46*(13), 7663–7671. https://doi.org/10.1029/2019GL083095

Labe, Z., Peings, Y., & Magnusdottir, G. (2020). Warm arctic, cold siberia pattern: Role of full Arctic amplification versus sea ice loss alone. *Geophysical Research Letters*, *47*(17), e2020GL088583. https://doi.org/10.1029/2020GL088583

Liang, Y.-C., Kwon, Y.-O., Frankignoul, C., Gastineau, G., Smith, K. L., Polvani, L. M., et al. (2023). The weakening of the stratospheric polar vortex and the subsequent surface impacts as consequences to Arctic sea-ice loss. *Journal of Climate*, *37*(1), 309–333. https://doi.org/10.1175/JCLI-D-23-0128.1

Lindgren, E. A., Sheshadri, A., & Plumb, R. A. (2018). Sudden stratospheric warming formation in an idealized general circulation model using three types of tropospheric forcing. *Journal of Geophysical Research: Atmospheres*, *123*(18), 125–210. https://doi.org/10.1029/2018JD028537

Matsuno, T. (1970). Vertical propagation of stationary planetary waves in the winter Northern Hemisphere. *Journal of the Atmospheric Sciences*, *27*(6), 871–883. https://doi.org/10.1175/1520-0469(1970)027⟨0871:VPOSPW⟩2.0.CO;2

McGraw, M. C., & Barnes, E. A. (2016). Seasonal sensitivity of the eddy-driven jet to tropospheric heating in an idealized AGCM. *Journal of Climate*, *29*(14), 5223–5240. https://doi.org/10.1175/JCLI-D-15-0723.1

McKenna, C. M., Bracegirdle, T. J., Shuckburgh, E. F., Haynes, P. H., & Joshi, M. M. (2018). Arctic Sea ice loss in different regions leads to contrasting Northern Hemisphere impacts. *Geophysical Research Letters*, *45*(2), 945–954. https://doi.org/10.1002/2017GL076433

Nakamura, T., Yamazaki, K., Iwamoto, K., Honda, M., Miyoshi, Y., Ogawa, Y., et al. (2016). The stratospheric pathway for Arctic impacts on midlatitude climate. *Geophysical Research Letters*, *43*(7), 3494–3501. https://doi.org/10.1002/2016GL068330

Orlanski, I., & Solman, S. (2010). The mutual interaction between external Rossby waves and thermal forcing: The subpolar regions. *Journal of the Atmospheric Sciences*, *67*(6), 2018–2038. https://doi.org/10.1175/2010JAS3267.1

Perlwitz, J., & Harnik, N. (2004). Downward coupling between the stratosphere and troposphere: The relative roles of wave and zonal mean processes. *Journal of Climate*, *17*(24), 4902–4909. https://doi.org/10.1175/JCLI-3247.1

Polvani, L. M., & Kushner, P. J. (2002). Tropospheric response to stratospheric perturbations in a relatively simple general circulation model. *Geophysical Research Letters*, *29*(7), 18-1. https://doi.org/10.1029/2001GL014284

Rantanen, M., Karpechko, A. Y., Lipponen, A., Nordling, K., Hyvärinen, O., Ruosteenoja, K., et al. (2022). The Arctic has warmed nearly four times faster than the globe since 1979. *Communications Earth and Environment*, *3*(1), 168. https://doi.org/10.1038/s43247-022-00498-3

Ring, M. J., & Plumb, R. A. (2007). Forced annular mode patterns in a simple atmospheric general circulation model. *Journal of the Atmospheric Sciences*, *64*(10), 3611–3626. https://doi.org/10.1175/JAS4031.1

Ring, M. J., & Plumb, R. A. (2008). The response of a simplified GCM to axisymmetric forcings: Applicability of the fluctuation-dissipation theorem. *Journal of the Atmospheric Sciences*, *65*(12), 3880–3898. https://doi.org/10.1175/2008JAS2773.1

Screen, J. A., Eade, R., Smith, D. M., Thomson, S., & Yu, H. (2022). Net equatorward shift of the jet streams when the contribution from sea-ice loss is constrained by observed eddy feedback. *Geophysical Research Letters*, *49*(23), e2022GL100523. https://doi.org/10.1029/2022GL100523

Screen, J. A., & Simmonds, I. (2010). The central role of diminishing sea ice in recent Arctic temperature amplification. *Nature*, *464*(7293), 1334–1337. https://doi.org/10.1038/nature09051

Screen, J. A., Simmonds, I., Deser, C., & Tomas, R. (2013). The atmospheric response to three decades of observed Arctic sea ice loss. *Journal of Climate*, *26*(4), 1230–1248. https://doi.org/10.1175/JCLI-D-12-00063.1

Sellevold, R., Sobolowski, S., & Li, C. (2016). Investigating possible Arctic-midlatitude teleconnections in a linear framework. *Journal of Climate*, *29*(20), 7329–7343. https://doi.org/10.1175/JCLI-D-15-0902.1

Sheshadri, A., Alan Plumb, R., & Gerber, E. P. (2015). Seasonal variability of the polar stratospheric vortex in an idealized AGCM with varying tropospheric wave forcing. *Journal of the Atmospheric Sciences*, *72*(6), 2248–2266. https://doi.org/10.1175/JAS-D-14-0191.1

Sheshadri, A., & Plumb, R. A. (2017). Propagating annular modes: Empirical orthogonal functions, principal oscillation patterns, and time scales. *Journal of the Atmospheric Sciences*, *74*(5), 1345–1361. https://doi.org/10.1175/JAS-D-16-0291.1

Sigmond, M., & Scinocca, J. F. (2010). The influence of the basic state on the Northern Hemisphere circulation response to climate change. *Journal of Climate*, *23*(6), 1434–1446. https://doi.org/10.1175/2009JCLI3167.1

Simpson, I. R., Blackburn, M., & Haigh, J. D. (2009). The role of eddies in driving the tropospheric response to stratospheric heating perturbations. *Journal of the Atmospheric Sciences*, *66*(5), 1347–1365. https://doi.org/10.1175/2008JAS2758.1

Simpson, I. R., & Polvani, L. M. (2016). Revisiting the relationship between jet position, forced response, and annular mode variability in the southern midlatitudes. *Geophysical Research Letters*, *43*(6), 2896–2903. https://doi.org/10.1002/2016GL067989

Smith, D. M., Eade, R., Andrews, M. B., Ayres, H., Clark, A., Chripko, S., et al. (2022). Robust but weak winter atmospheric circulation response to future Arctic sea ice loss. *Nature Communications*, *13*(1), 727. https://doi.org/10.1038/s41467-022-28283-y

Smith, D. M., Screen, J. A., Deser, C., Cohen, J., Fyfe, J., García-Serrano, J., et al. (2018). The polar amplification model Intercomparison Project (PAMIP) contribution to CMIP6: Investigating the causes and consequences of polar amplification. *Geoscientific Model Development*, *12*(3), 1–42. https://doi.org/10.5194/gmd-2018-82

Song, Y., & Robinson, W. A. (2004). Dynamical mechanisms for stratospheric influences on the troposphere. *Journal of the Atmospheric Sciences*, *61*(14), 1711–1725. https://doi.org/10.1175/1520-0469(2004)061⟨1711:DMFSIO⟩2.0.CO;2

Vallis, G. K., Colyer, G., Geen, R., Gerber, E., Jucker, M., Maher, P., et al. (2018). Isca, v1.0: A framework for the global modelling of the atmospheres of earth and other planets at varying levels of complexity [Software]. *Geoscientific Model Development*, *11*(3), 843–859. https://doi.org/10.5194/gmd-11-843-2018

Walz, R., Garny, H., Birner, T., & De, R. W. (2023). Stratospheric modulation of tropical upper-tropospheric warming-induced circulation changes in an idealized general circulation model. *Journal of the Atmospheric Sciences*, *80*(2), 611–631. https://doi.org/10.1175/JAS-D-21-0232.1

Weinberger, I., Garfinkel, C. I., Harnik, N., & Paldor, N. (2022). Transmission and reflection of upward-propagating Rossby waves in the lowermost stratosphere: Importance of the tropopause inversion layer. *Journal of the Atmospheric Sciences*, *79*(12), 3263–3274. https://doi.org/10.1175/JAS-D-22

Weinberger, I., Garfinkel, C. I., White, I. P., & Birner, T. (2021). The efficiency of upward wave propagation near the tropopause: Importance of the form of the refractive index. *Journal of the Atmospheric Sciences*, *78*(8), 2605–2617. https://doi.org/10.1175/JAS-D-20

Wu, Y., & Smith, K. L. (2016). Response of Northern Hemisphere midlatitude circulation to Arctic amplification in a simple atmospheric general circulation model. *Journal of Climate*, *29*(6), 2041–2058. https://doi.org/10.1175/JCLI-D-15-0602.1

Xu, M., Tian, W., Zhang, J., Screen, J. A., Huang, J., Qie, K., & Wang, T. (2021). Distinct tropospheric and stratospheric mechanisms linking historical Barents-Kara sea-ice loss and late winter Eurasian temperature variability. *Geophysical Research Letters*, *48*(20), e2021GL095262. https://doi.org/10.1029/2021GL095262

Xu, M., Tian, W., Zhang, J., Screen, J. A., Zhang, C., & Wang, Z. (2023). Important role of stratosphere-troposphere coupling in the Arctic mid-to-upper tropospheric warming in response to sea-ice loss. *npj Climate and Atmospheric Science*, *6*(1), 9. https://doi.org/10.1038/s41612-023-00333-2

Zhang, Y., Kong, Y., Yang, S., & Hu, X. (2023). Asymmetric Arctic and Antarctic warming and its intermodel spread in CMIP6. *Journal of Climate*, *36*(23), 8299–8310. https://doi.org/10.1175/JCLI-D-23-0118.1

Zheng, C., Wu, Y., Ting, M., Screen, J. A., & Zhang, P. (2023). Diverse Eurasian temperature responses to Arctic sea ice loss in models due to varying balance between dynamical cooling and thermodynamical warming. *Journal of Climate*, *36*(24), 8347–8364. https://doi.org/10.1175/jcli-d-22-0937.1